Journal of the Korean Physical Society, Vol. 76, No. 9, May 2020, pp. 802∼809

Study on the Energy Spectrum Response of a CdZnTe Detector

Yuandong Li,* Liangquan Ge, Kun Sun, Shangqing Sun, Guoqiang Zeng and Chengjun Tan
The College of Nuclear Technology and Automation Engineering, Chengdu University of Technology, Chengdu 610059, China

(Received 21 January 2020; revised 3 February 2020; accepted 19 February 2020)

In order to study the energy spectrum response of a CdZnTe detector, we firstly measured the temperature dependence and the bias dependence of the main characteristic parameters for both a quasi-hemispherical detector and a CAPture^{TM} plus detector. Secondly, we designed a low-noise readout circuit for the CdZnTe detector and measured the noise. Finally, we evaluated the energy spectrum response of the detector to different radioactive sources at different temperatures by connecting the detector to the readout circuit. The research showed that both detectors had low leakage current and junction capacitance, as well as good stability in temperature and bias; the quasi-hemispheric detector had a smaller leakage current and junction capacitance compared to the CAPture^{TM} plus detector; under zero input capacitor, the noise of the readout circuit was 612e, with the noise slope being 5.44e/pF; at room temperature(20 °C), the energy resolutions of the detector reached 3.84% and 1.36% for X-rays from ^{241}Am (59.5 keV) and gamma-rays from ^{137}Cs (662 keV), respectively; the signal-noise ratio of the output signal reached 31:1 with the rise time being 90 ns; at low temperature, the energy resolution reached 3.41% for the X-rays from ^{241}Am (59.5 keV); the detector achieved an excellent spectrum response and was able to distinguish clearly the energy peaks of ^{152}Eu and ^{226}Ra.

PACS numbers: 29.40.−n, 29.40.Wk
Keywords: CdZnTe detector, Characteristic parameter, Readout circuit, Output waveform, Energy spectrum response
DOI: 10.3938/jkps.76.802

I. INTRODUCTION

The CdZnTe detector is a new type of compound semiconductor detector with advantages such as high energy resolution, high intrinsic detection efficiency, high sensitivity, the ability to work at room temperature and insensitivity to humidity, overcoming the shortcomings of both scintillation detectors and high-purity germanium detectors in energy spectrum measurements [1,2]. Currently, with the growth technology of CdZnTe crystal being relatively mature [3,4], the application of the CdZnTe detector, which is a development trend in the future, has become a research hotspot [5–7]. The study of the energy spectrum response of the CdZnTe detector can provide a theoretical basis and technical support for its application in the fields such as nuclide recognition, radiation imaging, uranium exploration, high-energy physics and environmental monitoring. The main factors that affect the energy spectrum response are the stabilities of the characteristic parameters and the noise from the readout circuit [8].

Consequently, we carried out research on the energy spectrum response and compared the results with those for a quasi-hemispherical detector and a CAPture^{TM} plus CdZnTe detector. Firstly, we measured characteristic parameters such as the leakage current and the junction capacitance according to the principle of a unique variable at different temperatures and biases. Secondly, we designed a readout circuit with low noise and a folded structure for the detector and then measured the noise at different temperatures. Finally, we evaluated the energy spectrum response and the output waveform of the detector to a variety of radioactive sources by connecting the detector to the readout circuit at different temperatures, thus realizing a deep study of the basic physical characteristics of the CdZnTe detector and the design of front-end nuclear electronics, as well as the effect of the energy spectrum response. Considering the application environment for the CdZnTe detector, we set the bias range from 100 V to 400 V and the temperature range from −30 °C to 60 °C when measuring the leakage current. Because the junction capacitance, which only relates to the thickness of depletion zone and has little to do with temperature change, is an inherent property of the detector, we set the bias range from 50 V to 450 V and the temperature at 20 °C and −30 °C when measuring the junction capacitance. The main characteristics of the two detectors are shown in Table 1.

*E-mail: yuandongli@stu.cdut.edu.cn

Table 1. Characteristics of the two detectors.

Detector	Manufacturer	Size	Anode area	Growth method
Quasi-hemispherical detector	Northwestern Polytechnical University	4 mm × 4 mm × 2 mm	0.28 mm^2	Vertical Bridgman method
CAPture^{TM} plus detector	eV Company	4 mm × 4 mm × 2 mm	16 mm^2	High-pressure Bridgman method

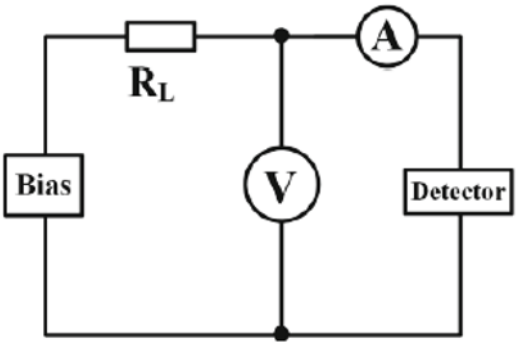

Fig. 1. Principle of the leakage current measurement.

II. CHARACTERISTIC PARAMETERS OF THE DETECTOR

1. Leakage Current Measurement

The leakage current, which relates to temperature and bias and determines the noise of the detector, is the stable current passing through the detector when it is not irradiated [9]. The principle of the leakage current measurement and the results are, respectively, shown in Fig. 1 and Fig. 2. The direct measured values of the leakage current are the readings of the high-sensitivity electrometer A when the detector is protected from light under a certain temperature and bias. During the measurement, the entire measurement device is electrically shielded, the detector is placed in a strictly dry environment, and the bias is slowly adjusted to avoid hysteresis.

Firstly, under the same bias, the leakage currents decrease obviously with decreasing temperature. When the temperature is low, the difference between the leakage currents of the two detectors is small. Therefore, an electric cooling sheet can be used to measure low-energy gamma rays. Secondly, at the same temperature, the leakage currents increase with increasing bias. The leakage currents of the quasi-hemispheric detector increase linearly with increasing bias and those of the CAPture^{TM} plus detector increase more obviously with increasing bias at a higher bias. Therefore, the bias voltage can be set as the value corresponding to the total depletion thickness of the detector. Thirdly, at the same bias voltage and temperature, the leakage current of the quasi-hemispheric detector is smaller than that of

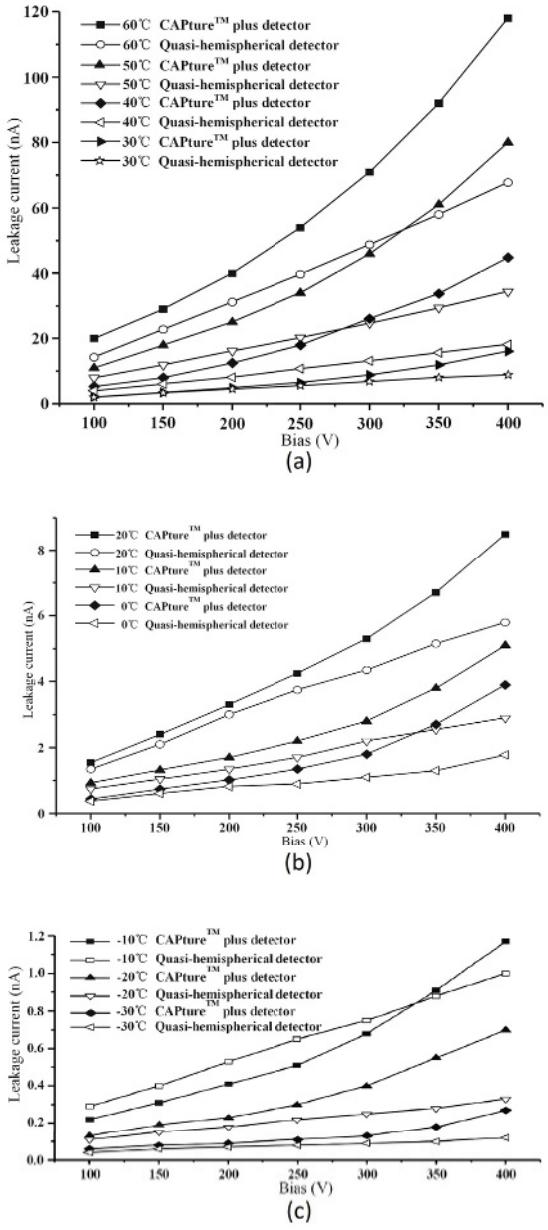

Fig. 2. Results of leakage current measurements at temperatures of (a) 60 – 30 °C, (b) 20 – 0 °C, and (c)−10 – −30 °C.

the CAPture^{TM} plus for two reasons. One is the difference between the electrode structures. The anode of the

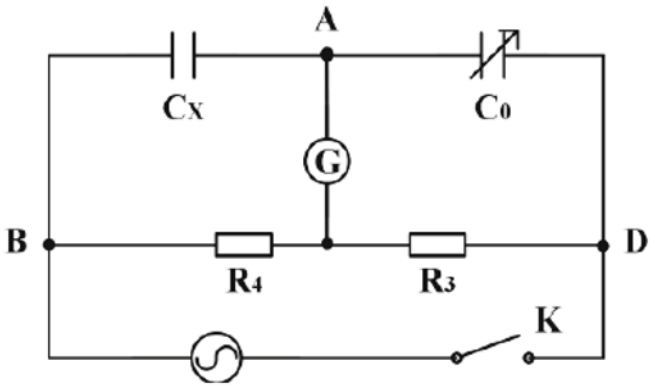

Fig. 3. Principle of the junction capacitance measurement.

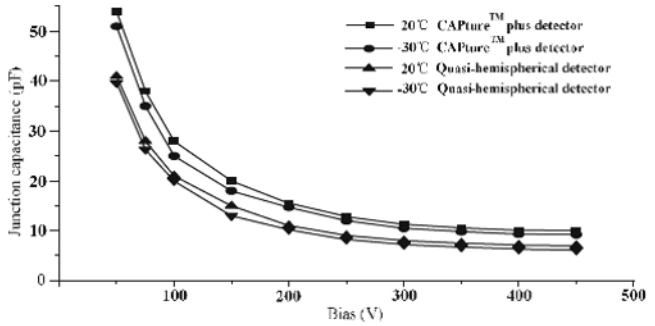

Fig. 4. Results of the junction capacitance measurements.

quasi-hemispherical detector is a dot with a diameter of 600 μm while that of the CAPture^{TM} plus detector is a bottom surface with an area of approximately 16 mm^2, so the latter has larger leakage current. The other is the difference between the methods used for the crystal growth and doping. With different dopings, the crystal of the quasi-hemispherical detector is grown through the vertical Bridgeman method while that of the CAPture^{TM} plus detector is grown through the high-pressure Bridgeman method. Finally, both detectors have comparatively small leakage current with good stability in temperature and bias; thus, the CdZnTe detector can be applied in X-ray detection systems with high energy resolution.

2. Junction Capacitance Measurement

The junction capacitance is the dielectric capacitance of the electrode and the semiconductor material [10]. The smaller the junction capacitance is, the larger the output pulse amplitude of the detector, the shorter the rise time, and the lower the noise are. The principle of the junction capacitance measurement is shown in Fig. 3. We used the arm-changing method of an alternating-current bridge to directly measure the junction capacitance. Thus, we were able to avoid the relative error caused by resistance. In the Fig. 3, R3 and R4 are known resistors; C0 is an adjustable standard capacitor; Cx is the capacitor to be measured; G is a balance indicator. Through derivation we can infer that

$$Cx = R3 \cdot C0 \cdot R4^{-1} . \quad (1)$$

$$Cd = C - C1 . \quad (2)$$

During the measurement, the measuring device is electrically insulated and dry, the frequency of the bridge signal is within the range from 10^5 to 10^6 Hz, and the signal is less than 10% of the bias, the bridge is considered to have reached equilibrium when the reading of the balance indicator can no longer decrease.

The results for the junction capacitance are shown in Fig. 4. Firstly, under the same bias, the junction capacitance is little affected by the temperature change. Secondly, at the same temperature, the junction capacitance decreases with increasing bias, and when the bias reaches a certain level (for example, 350 V), the junction capacitance reaches a small fixed value. Therefore, the bias value should be reasonable if the detector noise is to be reduced. Thirdly, at the same temperature and bias, the junction capacitance of the quasi-hemispherical detector is smaller than that of the CAPture^{TM} plus detector, which results from the difference between the electrode structure and the packaging technologies. Finally, both detectors have comparatively small junction capacitances with good stability in temperature and bias. In addition, under the same conditions, the quasi-hemispherical detector has a slightly smaller leakage current and junction capacitance as well as better performance, compared to the CAPture^{TM} plus detector. Thus, the follow-up research only focused on it.

III. DESIGN OF THE READOUT CIRCUIT

1. Design Principle

Considering the weak output signal [11], we designed a low-noise charge-sensitive amplifier with a folded structure as a readout circuit for the CdZnTe detector, as is shown in Fig. 5. In order to obtain a larger voltage signal, we employed three 0.1-pF capacitors connected in series as the feedback capacitor Cf. Thus, the charge sensitivity ACQ can be expressed as (R8 + R9) (R8·Cf)$^{-1}$ = 1.02 × 10^{14} V/C.

In order to couple the charge fully and reduce the low-frequency noise, we employed a 10-nF capacitor C1 as the AC coupling capacitor sharing the voltage with the readout circuit. The time constant $\tau 1$ of the discharge circuit, which is composed of R1 and C1, can be expressed as R1·C1 = 0.5 ms. Similarly, the time constant $\tau 2$ of the discharge circuit formed by the feedback resistor Rf (five 1 GΩ resistors in series) and Cf equals 0.167 ms, and the time constant $\tau 3$ of the differential molding circuit formed by C2 and R7 equals 3.2 μs, which is

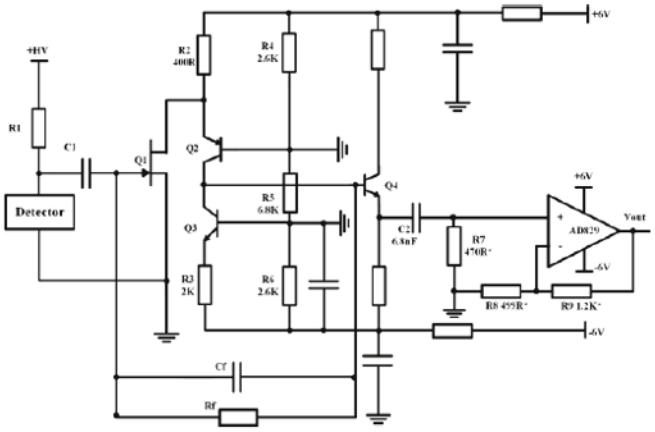

Fig. 5. Principle behind the readout circuit.

so much smaller than both $\tau 1$ and $\tau 2$ that no pole-zero can be produced. When the junction capacitance of the detector equals the common source input capacitance of the input stage Q1, the signal-to-noise ratio can reach its maximum, so we employed a junction field-effect transistor (2N4416) as Q1.

The bias circuit formed by resistors R4, R5, and R6 sets the static operating point. R6, R3, and transistor Q3 constitute a constant current source. The operating voltages of Q3 and R6 are 0.6 V and 2.6 V respectively, so the operating current of R3, Q3 and transistor Q2 is 1mA. R2, R4, and transistor Q2 constitute a constant current source guaranteeing that the current through R2 is 5 mA. Consequently, the current entering the drain of Q1 through R2 is 4 mA, which is within the range of the saturated drain current and sets the drain voltage of Q1 to 4 V to reduce the noise of Q1. R6, R3, and Q3 form a constant current source as an active load for Q2 to improve the open-loop gain of the circuit.

The signal passing through Q4 is amplified by using a common-collector in order to improve the signal-to-noise ratio. Because $\tau 1$ and $\tau 2$ are large, amplifying the signal directly will lead the output of the amplifier to a full-amplitude overload at a high counting rate. Therefore, the signal passes through a differential shaping circuit composed of C2 and R7 first and is then amplified by an AD829 operational amplifier [12].

2. Noise Measurement

The equivalent noise charge of the readout circuit is measured according to the measurement method recommended by the International Electrotechnical Commission [13]. We firstly placed the readout circuit in a metal shield with all input ends and output ends passing through the BNC interface in order to shield the interference from the measurement environment. We then placed a metal shield in a constant temperature box.

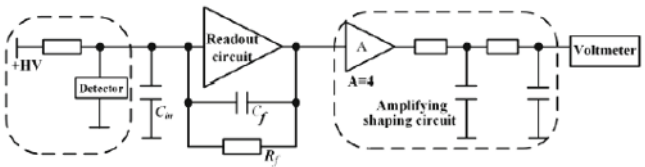

Fig. 6. Measurement schematic for equivalent noise charge.

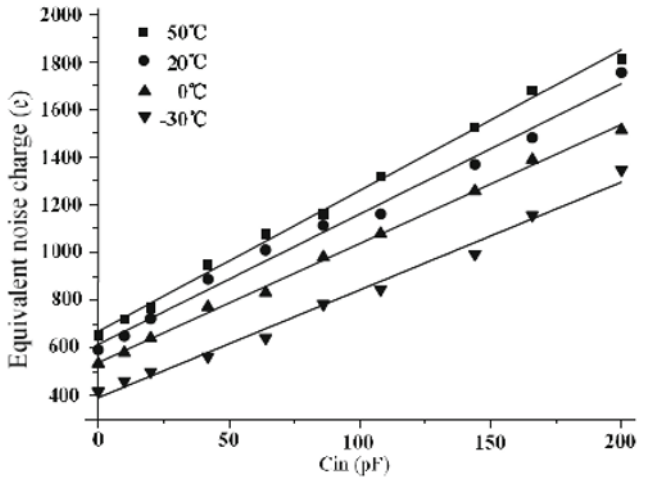

Fig. 7. Relationship between equivalent noise charge and Cin.

The measurement schematic is shown in Fig. 6.

When no signal input exits, the root-mean-square value V_{no} of the output voltage is measured, and the noise linewidth $\mathrm{FWHM_{NV}}$ in voltage can be expressed as

$$FWHM_{\mathrm{NV}} = 2.355 V_{\mathrm{no}}. \tag{3}$$

After some deduction, the equivalent noise $\mathrm{FWHM_{Ne}}$ in electrons can be expressed as

$$FWHM_{\mathrm{Ne}} = 2.355 V_{\mathrm{no}} \cdot (A_{\mathrm{CQ}} \cdot q)^{-1}. \tag{4}$$

In order to evaluate the noise, we firstly disconnected the detector from the readout circuit and set the time constant of the amplifying shaping circuit to be the same as that of the differential shaping circuit composed of C2 and R7. Next, we changed the capacitance $\mathrm{C_{in}}$ of the readout circuit input end at different temperatures (50 °C, 20 °C, 0 °C and − 30 °C) and finally converted V_{no} to an equivalent noise charge. We then plotted the relationship between the equivalent noise charge and $\mathrm{C_{in}}$ in Fig. 7. At room temperature, the noise of the readout circuit is 612e under zero input capacitor, with the noise slope being 5.44e/pF; at −30 °C, the noise is 383e under zero input capacitor, with the noise slope being 4.52e/pF. The noise of readout circuit can be seen to be effectively reduced by lowering the temperature.

In order to measure the relationship between the equivalent noise charge and the time constant at different

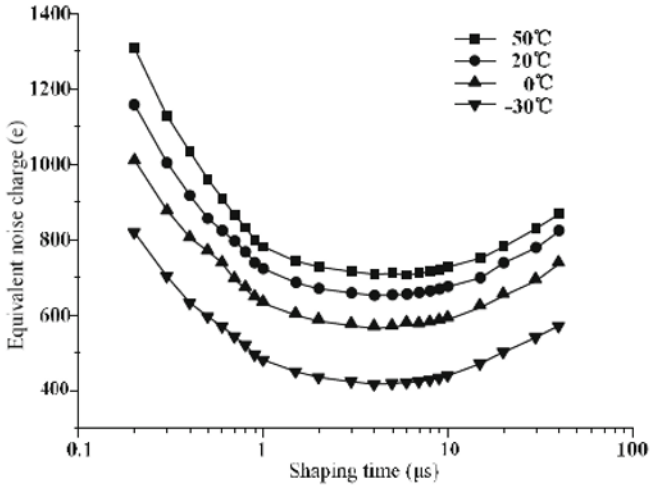

Fig. 8. Relationship between equivalent noise charge and the shaping time constant.

temperatures, we connected the detector to the readout circuit and then changed the time constant of the amplifying shaping circuit continuously. The results are shown in Fig. 8. At different temperatures, the readout circuit has lower noise when the time constant of the amplifying shaping circuit is set from 1 to 20 μs, thus indicating that the time constant of the next stage multichannel analyzer should be set within the range from 1 to 20 μs.

In addition, the average ionization energy of CdZnTe detector is about 5 eV, so the detector can generate about 1180e for the X-rays from ^{59}Fe (5.9 keV). Because the junction capacitance of detector is about 8 pF and the noise of the readout circuit is about 427e at −30 °C, we can infer from above results that the detector has the ability to detect X-rays from ^{59}Fe effectively, thus providing a research basis for the application of CdZnTe detectors in low-energy X-ray detection.

IV. ENERGY SPECTRUM RESPONSE AND APPLICATION

1. Energy Spectrum Response to Low-Energy X-rays

We adopted ^{241}Am (59.5 keV) to measure the energy spectrum response from low-energy X-rays. We firstly connected the detector to the readout circuit and placed them inside a metal shield. Then, we opened a small square hole with an area of 4 × 4 mm^2 on the shield and pasted an aluminized film on the shield to reduce the absorption of X-rays. Finally, we placed the ^{241}Am facing the detector at a separation of 5 cm. During the measurement, we set the measurement time to 100 s, the temperature at 20 °C, the bias to 300 V, and the shaping time to 1.5 μs. The energy spectrum measured using a multichannel analyzer is shown in Fig. 9, with the resolution being 2048. At room temperature, the resolution can reach 3.84% for X-rays from ^{241}Am (59.5 keV), thus providing a research basis for the development of a high-resolution X-ray detection system.

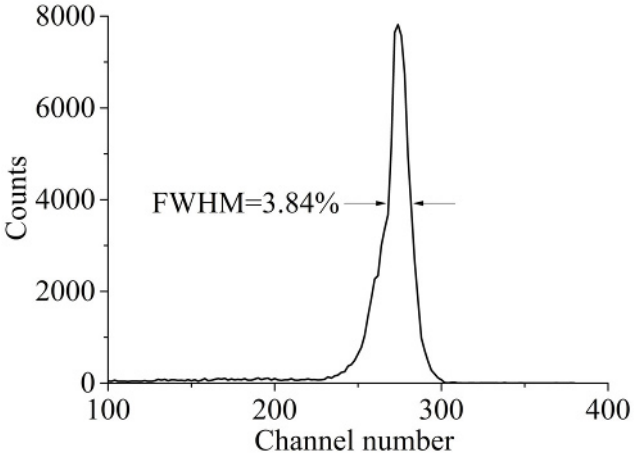

Fig. 9. Energy spectrum of ^{241}Am.

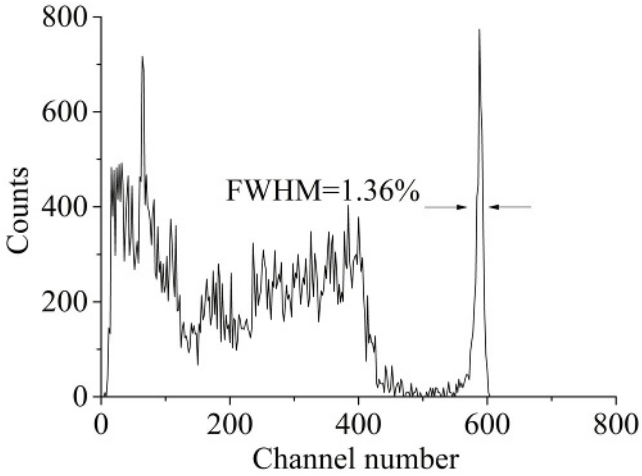

Fig. 10. Energy spectrum of ^{137}Cs.

2. Energy Spectrum Response to High-Energy Gamma-rays

We adopted ^{137}Cs (662 keV) to measure the energy spectrum response of high-energy gamma-rays. Because the CdZnTe detector suffers from low detection efficiency for high-energy gamma-rays, we had to prolong the measurement time appropriately. Using a method similar to that mentioned above, we set the measurement time to 30 minutes and the bias to 350 V, with other experimental conditions unchanged. The energy spectrum is shown

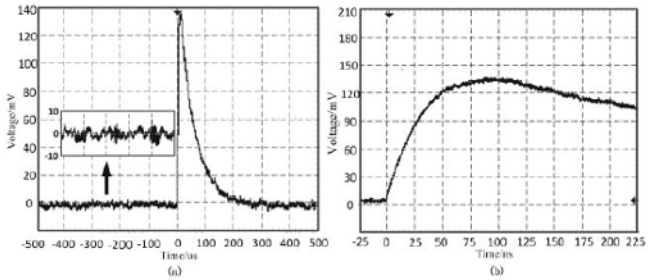

Fig. 11. Output waveform.

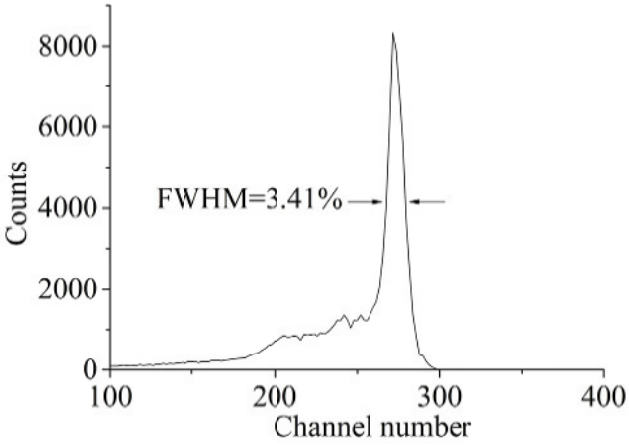

Fig. 12. Energy spectrum of ^{241}Am at −20 °C.

in Fig. 10. The resolution of detector reaches 1.36% for ^{137}Cs. The detector has more advantages for high-energy gamma-ray measurements, which is determined by the electrode structure of the detector. The anode of the quasi-hemispherical detector is a dot with a diameter of 600 μm, and the cathode is composed of the top surface and four side faces, thus leading to a small charge capture effect of the detector and better peak shape as shown in Fig. 10, providing a research basis for the development of a high-energy gamma-ray measurement system.

3. Output Waveform

We connected the readout circuit to the detector and put them in a metal shield, after which we measured the output waveform of the gamma-rays from ^{137}Cs by using an oscilloscope. The results are shown in Fig. 11. According to Fig. 11(a), the root-mean-square value of the equivalent noise is 4.4 mV, the pulse amplitude is 137 mV, and the signal-to-noise ratio is as high as 137/4.4 ≈ 31:1. The frequency characteristic of the detector can be evaluated by using the rise time of the signal. According to Fig. 11(b), the rise time is 90 ns, indicating that the detector has excellent output frequency characteristic.

Fig. 13. Nuclide identification instrument.

4. Energy Spectrum Response at Low Temperature

Lowering the temperature can reduce both the leakage current of the detector and the noise of the readout circuit, which can improve the overall system performance. We adopted ^{241}Am (59.5 keV) to measure the energy spectrum response and set the temperature at −20 °C. The result is shown in Fig. 12. The energy resolution of the detector can be seen to have been improved from 3.84% to 3.41% at room temperature, with reduced noise of 256e, thus providing a research basis for the development of an X-ray fluorescence logging instrument.

5. Applications

Common nuclide recognition detectors include NaI (Tl) detectors and $LaBr_3$ (Ce) detectors [14], but the NaI (Tl) detector suffers from poor energy resolution, and the $LaBr_3$ (Ce) detector suffers from strong interference generated by inherent nuclides (^{138}La and ^{227}Ac) [15]. According to the above research results, the CdZnTe detector has many advantages, such as high energy resolution, small size, the ability to measure broad energies, good detection efficiency and energy resolution, and the ability to work at room temperature, thus making it good for detecting both low-energy X-rays and middle-energy X-rays with a broad prospect in nuclide identification applications. The real object of a nuclide identification system based on the CdZnTe detector developed in this paper is shown in Fig. 13.

^{152}Eu and ^{226}Ra were adopted to evaluate the detector's capability to identify nuclides. ^{152}Eu can emit gamma-rays with many energy: 121.8 keV, 244.7 keV, 344.3 keV, 778.9 keV, 964.1 keV, 1085.8 keV, 1112.1 keV,

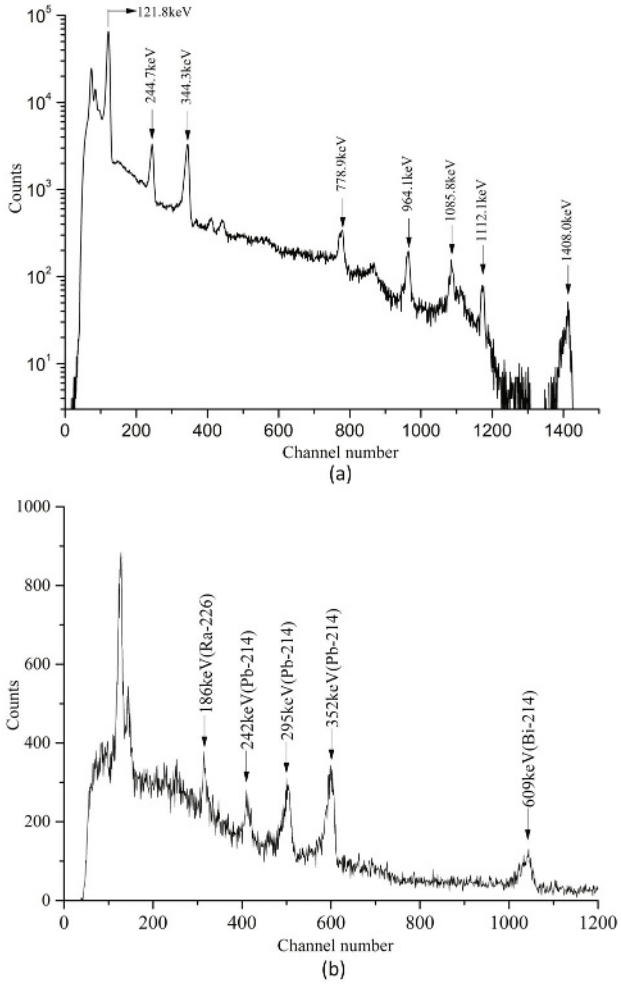

Fig. 14. Energy spectra of (a) ^{152}Eu and (b) ^{226}Ra.

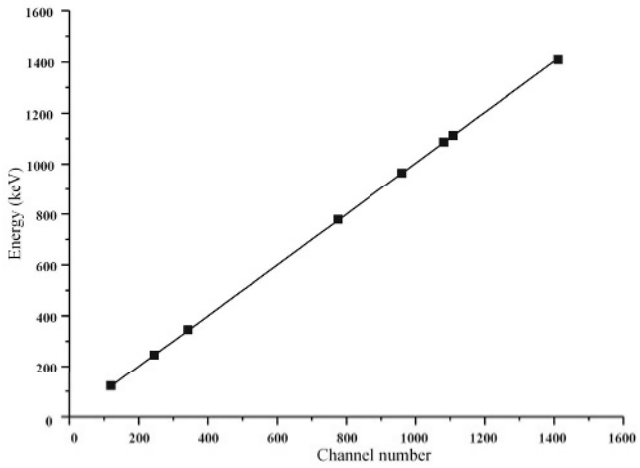

Fig. 15. Line fitting to the energy vs. channel number data.

and 1408.0 keV. ^{226}Ra can emit gamma-rays with an energy of 186 keV, and its one decay daughter ^{214}Pb can emit gamma-rays with energies of 242 keV, 295 keV and 352 keV; another decay daughter ^{214}Bi can emit gamma-rays with an energy of 609 keV [16]. Thus, the nuclide recognition ability of the CdZnTe detector can be evaluated by using these two radioactive sources.

During the measurement, we placed the three radioactive sources facing the detector at a distance of 5 cm. We prolonged the measurement time to 150 minutes to obtain more counts and set the measurement temperature to room temperature, the bias to 380 V, and the shaping time to 1.5 μs. Next, we evaluated the energy spectrum response and finally fitted the peak position of ^{152}Eu to the channel number linearly. The results are shown in Fig. 14 and Fig. 15. The detector can be seen to achieve a high resolution for high-energy gamma-rays and an excellent, linear energy spectrum response reaching 0.9999, making it easy to distinguish between the energies of ^{152}Eu and ^{226}Ra clearly. In addition, because of the limitation of the budget, the size of the adopted detector is merely $4 \times 4 \times 2$ mm^3. If we adopt a CdZnTe detector with a size of $10 \times 10 \times 10$ mm^3, the detection efficiency should increase 31.25 times, thus shortening the experimental time to 4.8 minutes.

V. CONCLUSION

Our research shows that both CdZnTe detectors have small leakage current, small junction capacitance, and good stability in temperature and bias. Under the same conditions, the quasi-hemispheric detector has a smaller leakage current, a smaller junction capacitance, and better performance compared to the CAPture^{TM} plus detector. The designed readout circuit has low noise and good performance; the detector achieves high energy resolution and high energy linearity for both low-energy X-rays and high-energy gamma-rays. The detector has a good energy spectrum response at room temperature. At low temperature, its performance will be further enhanced, making possible its wide application.

ACKNOWLEDGMENTS

The authors acknowledge the financial support by the National Key R&D Program of China (Project No.2017YFC0602105), and the National Science Foundation of China (Project No. 41774147, Project No. 41774190 and Project No. 41804114).

REFERENCES

[1] D. Goodman *et al.*, IEEE Trans. Nucl. Sci. **64**, 2531 (2017).
[2] M. B. Tzolov, N. C. Barbi, C. T. Bowser and O. E. Healy, Microsc. Microanal. **22**, 594 (2016).

[3] C. Henager *et al.*, J. Electron. Mater. **44**, 1 (2015).
[4] I. D. Burlakov *et al.*, J. Commun. Technol. Electron. **61**, 333 (2016).
[5] M. D. Wilson *et al.*, Nucl. Instrum. Methods Phys. Res. A **652**, 158 (2011).
[6] V. M. Sklyarchuk, V. A. Gnatyuk and W. Pecharapa, Nucl. Instrum. Methods Phys. Res. A **879**, 101 (2018).
[7] S. D. Sordo *et al.*, Sensors **9**, 3491 (2009).
[8] M. Amman *et al.*, IEEE Trans. Nucl. Sci. **56**, 795 (2014).
[9] U. Otuonye, H. W. Kim and W. D. Lu, Appl. Phys. Lett. **110**, 173104 (2017).
[10] S. Kalbitzer and W. Melzer, Nucl. Instrum. Methods **56**, 301 (1967).
[11] J. C. Kim, W. R. Kaye and Z. He, J. Korean Phys. Soc. **64**, 1336 (2014).
[12] Y. D. Li *et al.*, At. Energy Sci. Technol. **51**, 1741 (2017).
[13] V. Radeka *et al.*, IEEE Trans. Nucl. Sci. **35**, 155 (1988).
[14] I. Meleshenkovskii *et al.*, EPJ Web Conf. **170**, 07007 (2018).
[15] G. Cozzi *et al.*, IEEE Trans. Nucl. Sci. **65**, 645 (2017).
[16] H. Schrader, Appl. Radiat. Isot. **114**, 202 (2016).